Carrier-wave Rabi flopping on radiatively coupled shallow donor transitions in *n*-type GaAs

P. Gaal,[1] W. Kuehn,[1] K. Reimann,[1,*] M. Woerner,[1,†] T. Elsaesser,[1] R. Hey,[2] J. S. Lee,[3] and Ulrich Schade[3]
[1]*Max-Born-Institut für Nichtlineare Optik und Kurzzeitspektroskopie, 12489 Berlin, Germany*
[2]*Paul-Drude-Institut für Festkörperelektronik, 10117 Berlin, Germany*
[3]*Berliner Elektronenspeicherring-Gesellschaft für Synchrotronstrahlung mbH, 12489 Berlin, Germany*
(Received 31 October 2007; revised manuscript received 18 March 2008; published 9 June 2008)

Ultrafast phase-resolved terahertz propagation experiments reveal the nonlinear optical response of shallow donor transitions in *n*-type GaAs. At a lattice temperature of 100 K, carrier-wave Rabi oscillations between bound impurity levels govern the nonlinear terahertz response for terahertz driving fields up to 5 kV/cm. The radiative coupling between impurity transitions results in a coherently excited macroscopic $1S$-$2P$ polarization that oscillates for several picoseconds. A comparison with the Bloch equations for radiatively coupled two-level systems demonstrates a breakdown of the two-level approach for field amplitudes above 5 kV/cm.

DOI: 10.1103/PhysRevB.77.235204 PACS number(s): 78.47.−p, 71.55.Eq, 42.65.Re

I. INTRODUCTION

A shallow donor impurity in a doped semiconductor resembles a hydrogen atom in many aspects. Compared to an atom, however, the values of relevant physical quantities, such as the binding energy E_{1S}, the effective Bohr radius a_B^*, and the transition dipole moments between bound states, differ by orders of magnitude. Si donors in GaAs, an important model system, display a binding energy $E_{1S}=6$ meV$=h\times 1.5$ THz (h, Planck's constant), an effective Bohr radius $a_B^*=10$ nm, and an internal electric field $F_0=E_{1S}/(ea_B^*)=6$ kV/cm. These large differences are caused by the small effective mass ($m^*=0.067m_0$) and the large static dielectric constant ($\epsilon_s=12.4$) of GaAs. The comparably small internal electric field makes nonlinear quantum manipulations with high-field terahertz pulses[1] possible, e.g., Rabi oscillations[2] in high magnetic fields and at low donor concentrations ($N_D=3\times 10^{14}$ cm^{-3}) or terahertz-field-induced impurity ionization followed by radiative recombination[3] at high donor concentrations ($N_D=10^{17}$ cm^{-3}).

At very low doping concentrations ($N_D\lesssim 10^{14}$ cm^{-3}), the impurities are nearly isolated. For these concentrations, one observes a hydrogenlike absorption spectrum of neutral shallow donors exhibiting at low temperatures a very sharp $1S$-$2P$ transition line at 1.1 THz (red/gray dashed line in Fig. 1).[4] Studies at low temperatures in the terahertz range[5–7] have revealed nanosecond population lifetimes and picosecond decoherence times of coherent polarizations of bound donor electron states. These properties make possible far-infrared lasing on donor transitions[8] in Si and make donors candidates for charge qubits in quantum information processing.[2,9–11] With increasing doping concentration, one expects the $1S$-$2P$ transition to broaden because individual neutral donors interact with each other. As we will show, even at doping concentrations of the order of the Mott density [Eq. (2) in Ref. 12] ($N_D\approx 1\times 10^{16}$ cm^{-3}), as in our sample studied here, there exist sharp $1S$-$2P$ absorption lines, which exhibit long-lasting optical coherences.

In this paper, we study the nonlinear terahertz response of *n*-type bulk GaAs with a donor concentration of $N_D=2\times 10^{16}$ cm^{-3} at a lattice temperature of $T=100$ K. The emitted terahertz radiation is directly measured in phase-resolved nonlinear propagation experiments for applied terahertz field amplitudes between 0.6 and 17 kV/cm. We observe long-lived optical coherences due to the radiative coupling and carrier-wave Rabi oscillations between bound states of shallow donors. A comparison with theory, i.e., with the Bloch equations for radiatively coupled two-level systems, shows that the Rabi oscillation picture holds for driving fields up to 5 kV/cm, while for higher terahertz fields the two-level ap-

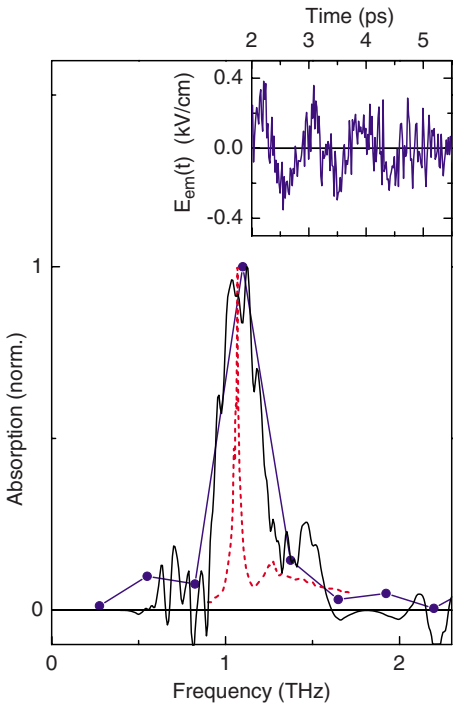

FIG. 1. (Color online) Normalized linear absorption spectra of *n*-type GaAs. The solid black line shows the linear absorption spectrum of our sample ($N_D=2\times 10^{16}$ cm^{-3}) measured in a Fourier-transform spectrometer at a temperature of $T=27$ K. The blue/dark gray dots are the Fourier transform of the time-resolved free-induction decay (the electric field transient measured after the excitation pulse, shown in the inset) of the sample at $T=100$ K. For comparison, the red/gray dashed line shows the photoconductivity spectrum of nearly isolated donor impurities ($N_D=3\times 10^{13}$ cm^{-3}) measured at $T=4.2$ K (data taken from Ref. 4).

proach breaks down and the field ionization processes of the neutral impurities come into play.

II. EXPERIMENT

The linear terahertz absorption of our sample was measured at different lattice temperatures with a Fourier-transform far-infrared spectrometer (spectral resolution 0.15 THz). In the nonlinear experiments, a few-cycle terahertz pulse with a center frequency of 2 THz interacts with the semiconductor sample. The transmitted terahertz field is measured in amplitude and phase by electro-optic sampling[13] in a thin ZnTe crystal. Details of the terahertz generation and the experimental setup have been previously described.[3,14] The entire optical path of the terahertz beam is placed in vacuum to suppress any influence of spurious gas absorption or emission on the measured signal. The sample investigated here was grown by molecular beam epitaxy on a semi-insulating GaAs substrate and consists of a 500 nm thick layer of Si-doped GaAs (doping concentration $N_D=2\times10^{16}$ cm^{-3}) clad between two 300 nm thick $Al_{0.4}Ga_{0.6}As$ barrier layers. For the nonlinear propagation studies, the substrate was removed by wet chemical etching.[15]

III. RESULTS AND DISCUSSION

A. Linear terahertz absorption

In Fig. 1, we present the normalized linear absorption spectrum of our sample measured at $T=27$ K (black solid line). The strong absorption line is attributed to the $1S$-$2P$ transition of the Si donor atoms. Measurements at $T=100$ K (not shown) reveal an identical spectral envelope with a peak absorption that is only 10% less than at 27 K. Compared to samples of much lower doping concentration, i.e., to isolated impurities[4] (red/gray dashed line), the center of gravity of this line is slightly shifted toward higher frequencies (1.2 vs 1.1 THz) with a substantially larger spectral width (full width at half maximum 0.3 vs 0.03 THz). A major fraction of the additional linewidth originates from the limited spectral resolution of the Fourier-transform spectrometer. For comparison with such linear absorption spectra, we plot the Fourier transform (blue/dark gray dots) of the time-resolved free-induction decay (inset of Fig. 1) measured in our nonlinear experiments.

The doping concentration $N_D=2\times10^{16}$ cm^{-3} of our sample is of the order of the Mott density[12] at which a pronounced coupling of impurities exists. In view of this fact, the observed spectral width of absorption is surprisingly low. The following mechanisms are relevant for understanding the origin of the rather narrow line:

(i) For intermediate and high doping concentration, the electron in a particular donor atom sees not only the Coulomb potential of this donor but also the Coulomb potentials of positively charged nuclei of other donors in its vicinity. This leads to the formation of impurity bands,[16] i.e., to a distribution of transition frequencies.

(ii) The electron interacts with other bound and free electrons in the vicinity.

(iii) In a dense ensemble of identical atoms, radiative coupling of optical transitions on different atoms occurs. The radiation field acting on a particular atom is the sum of the externally applied field and the radiation reaction fields of all the atoms in its neighborhood. The relevant sample volume is of the order of λ^3 (λ, wavelength of the optical transition). In the terahertz spectral range, radiative coupling is particularly important because of the long wavelengths involved. It can easily overcome the decoherence rate of individual transitions resulting in long-lived macroscopic optical polarizations. In that case the linewidth is essentially determined by radiative damping of the optical transition. In semiconductors, such nonlinear radiative coupling effects have been observed for both interband[17,18] and intersubband[19] transitions. However, this effect has been neglected in the analysis of far-infrared absorption spectra of n-type GaAs so far.[20]

The interplay of such mechanisms determines the overall line shape of absorption. Presently, there exists no theoretical approach to describe such complex many-body effects in a consistent and quantitative way. In the Appendix, we present qualitative arguments for narrow $1S$-$2P$ absorption lines at doping concentrations of the order of the Mott density.[12]

The moderate 10% decrease of the peak absorption when heating the sample from 27 to 100 K also points to the relevance of many-body effects for linear absorption. In a single particle picture assuming a two-level dipole transition at 1.2 THz, one expects a much stronger decrease of absorption of 64% for a temperature increase from 27 to 100 K, originating from the decrease of the thermal population difference of the two levels.

B. Nonlinear terahertz propagation

Terahertz transients measured at $T=100$ K over a broad range of terahertz electric field amplitudes are presented in Figs. 2 and 3. In Fig. 2(a), the electric fields of the incident pulse $E_{in}(t)$ (blue/dark gray dashed line) with a peak amplitude of 15 kV/cm and of the transmitted pulse $E_{tr}(t)$ (black dash-dotted line) are plotted as a function of time. As the thickness of our sample $d=500$ nm is much less than the terahertz wavelength $\lambda\approx150$ μm, all donor atoms in the sample experience the same driving field $E_{loc}(t)$, which is identical to the terahertz field $E_{tr}(t)$ [inset of Fig. 2(a)] transmitted through the sample.[17,19] In such thin-film geometry, the field coherently emitted by the sample [red/gray solid line in Fig. 2(a)] is given by the difference $E_{em}(t)=E_{tr}(t)-E_{in}(t)$. Since a thin film equally emits in both directions, the reflected field is equal to the emitted field, $E_{re}(t)=E_{em}(t)$.

The phase relation between the emitted field $E_{em}(t)$ and the driving field $E_{loc}(t)=E_{tr}(t)$ changes with time: During the first period of $E_{loc}(t)$, the emitted field is of opposite phase ($\Phi=\pi$), followed by the second period where the two fields are in phase ($\Phi=0$). Such highly nonlinear behavior corresponds to an absorptive response during the first period and to stimulated emission during the second period.[21] In a more quantitative way, we calculated the time-dependent energy transfer rate to the sample $I_{abs}(t)$ as the difference between the incident intensity and the sum of the transmitted and reflected intensities. The intensities outside the sample, i.e.,

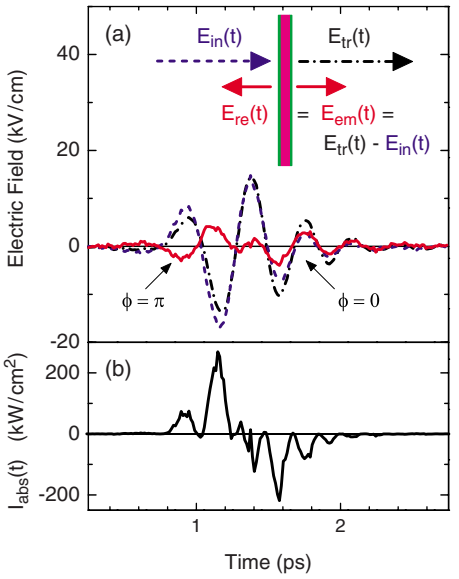

FIG. 2. (Color online) (a) Nonlinear propagation of a high-field terahertz transient through an *n*-type GaAs layer at a temperature of 100 K. The electric field is plotted as a function of time for the incident pulse $E_{\mathrm{in}}(t)$ (dashed line) and for the transmitted pulse $E_{\mathrm{tr}}(t)$ (dash-dotted line). Inset: in the thin-film geometry the coherently emitted field (solid line) is the difference $E_{\mathrm{em}}(t)=E_{\mathrm{tr}}(t)-E_{\mathrm{in}}(t)$. The time-dependent phase relation between $E_{\mathrm{em}}(t)$ and $E_{\mathrm{tr}}(t)$ indicates absorptive ($\Phi=\pi$) and stimulated-emission-like ($\Phi=0$) phases of the sample-terahertz-field interaction. (b) Time-dependent energy absorption of the sample $I_{\mathrm{abs}}(t)=-2\epsilon_0 cE_{\mathrm{em}}(t)E_{\mathrm{tr}}(t)$.

in vacuum, are given by $\epsilon_0 cE^2$. Thus, $I_{\mathrm{abs}}(t)=\epsilon_0 c[E_{\mathrm{in}}(t)^2-E_{\mathrm{re}}(t)^2-E_{\mathrm{tr}}(t)^2]=-2\epsilon_0 cE_{\mathrm{em}}(t)E_{\mathrm{tr}}(t)$, as shown in Fig. 2(b). The energy absorbed during the first terahertz period is almost completely reemitted in the second period. The fact that the maxima and minima of $I_{\mathrm{abs}}(t)$ occur at the same times as the peaks of the driving field amplitude $|E_{\mathrm{loc}}(t)|$ points to a resonant energy exchange between the sample and the terahertz field.

Data for lower peak amplitudes of the driving field are summarized in Fig. 3, displaying the emitted field transients $E_{\mathrm{em}}(t)$ (thin black lines) measured for amplitudes of the exciting terahertz field E_{in} between 0.6 and 10 kV/cm. The temporal shape of the driving field $E_{\mathrm{in}}(t)$ (dashed blue/dark gray line) is identical for all field amplitudes. Up to an amplitude of $E_{\mathrm{in}}\approx 1.5$ kV/cm, the data reveal a strictly linear response of the sample to the driving field. Starting with $E_{\mathrm{in}}=1.7$ kV/cm (not shown), the response $E_{\mathrm{em}}(t)$ becomes nonlinear, showing a strongly varying temporal shape [Figs. 3(c)–3(e)]. In particular, one observes a pronounced saturation of the amplitude of the emitted field, which is limited to values $|E_{\mathrm{em}}(t)|<0.5$ kV/cm. During the excitation pulse, the emission transients in Figs. 3(c)–3(e) exhibit oscillations with a frequency around the third harmonic of $E_{\mathrm{in}}(t)$, a clear signature of carrier-wave Rabi oscillations.[22–24] In addition, the emitted field shows strong coherent oscillations well after the driving pulse ($t>2$ ps). This long-lasting coherence points to a collective behavior of the emitting dipoles, which is fully reproduced by our model calculations (thick red/gray lines).

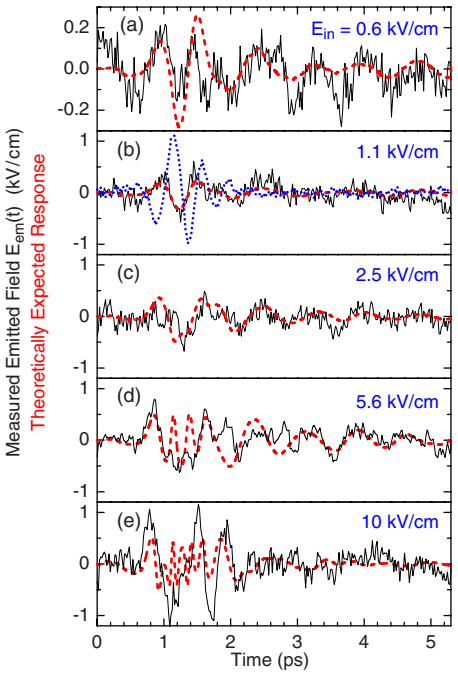

FIG. 3. (Color online) Measured emitted field transients $E_{\mathrm{em}}(t)=E_{\mathrm{tr}}(t)-E_{\mathrm{in}}(t)$ (black solid lines) for different amplitudes of the exciting terahertz field $E_{\mathrm{in}}(t)$. The form of $E_{\mathrm{in}}(t)$ is shown in (b) as the blue/dark gray dotted line. Red/gray dashed lines: theoretically predicted $E_{\mathrm{em}}(t)$ on the basis of the Bloch equations describing radiatively coupled two-level systems.

Figures 4(a), 4(c), and 4(e) show the time-dependent rate $I_{\mathrm{abs}}(t)=-2\epsilon_0 cE_{\mathrm{em}}(t)E_{\mathrm{tr}}(t)$ of coherent energy transfer to the sample derived from the transients $E_{\mathrm{em}}(t)$ in Figs. 3(b)–3(d). For a more detailed analysis of the data, we calculate the energy per electron $\Lambda(t)$ that is transiently deposited in the sample:

$$\Lambda(t)=\frac{1}{N_D d}\int_{-\infty}^{t} I_{\mathrm{abs}}(t')dt'. \tag{1}$$

Figures 4(b), 4(d), and 4(f) show $\Lambda(t)$ calculated from the transients in Figs. 4(a), 4(c), and 4(e) (black lines). The thick red/gray lines are the results of the theoretical model discussed below. We find an increase of the energy content of the sample during the first period of the terahertz driving pulse and a decrease to values close to zero during the second period. In the linear case [Figs. 4(a) and 4(b)], $I_{\mathrm{abs}}(t)$ oscillates around zero due to the slightly off-resonant center frequency (≈ 2 THz) of the driving pulse compared to the $1S$-$2P$ transition frequency (≈ 1.2 THz). Correspondingly, the transiently stored energy $\Lambda(t)$ increases with strong oscillations as a function of time. For $E_{\mathrm{in}}<5$ kV/cm [panels (b) and (d)], the energy deposited per electron is below the transition energy, i.e., $\Lambda(t=1.25\ \mathrm{ps})<\hbar\omega_{1S\text{-}2P}=5$ meV [see dotted lines in Figs. 4(b), 4(d), and 4(f)]. Thus, ionization of the donors by the terahertz field is negligible in this range of driving fields.

We analyze our experimental results with theoretical calculations of the coherent response of electrons bound to shallow donors. In the most elementary approach, Rabi oscilla-

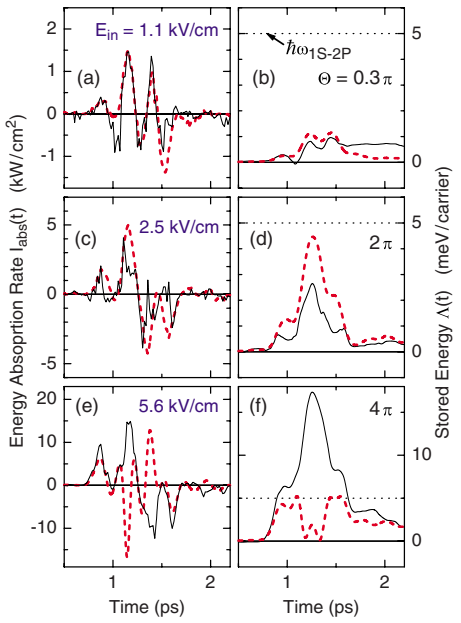

FIG. 4. (Color online) Left panels: time-dependent intensity $I_{\mathrm{abs}}(t)=-2\epsilon_0 cE_{\mathrm{em}}(t)E_{\mathrm{tr}}(t)$ (black solid lines, experiment; red/gray dashed lines, theory) of the coherent energy transfer to the sample corresponding to transients of panels (b), (c), and (d) in Fig. 3, respectively. Right panels: corresponding values of the transiently stored energy per electron $\Lambda(t)$ [see Eq. (1)]. In the theory (red/gray dashed lines), i.e., in the Bloch equations for a two-level system, this magnitude equals the time-dependent excited state population $\rho_{22}(t)$ multiplied by the transition energy $\hbar\omega_{1S\text{-}2P}$ for Rabi oscillations with pulse areas of $\Theta=0.3\pi$, 2π, and 4π, respectively. The dotted lines show $\hbar\omega_{1S\text{-}2P}$.

tions of the polarization amplitude and of the population inversion are predicted by the Maxwell-Bloch equations for two-level systems:[17,21,25]

$$\frac{\partial\rho_{12}}{\partial t}=\left(i\omega_{1S\text{-}2P}-\frac{1}{T_2}\right)\rho_{12}+i\Omega(t)(1-2\rho_{22}),$$

$$\frac{\partial\rho_{22}}{\partial t}=-\frac{1}{T_1}\rho_{22}+2\Omega(t)\mathrm{Im}(\rho_{12}),$$

$$P=2N_D d\mu_{1S\text{-}2P}\,\mathrm{Re}(\rho_{12}),$$

$$E_{\mathrm{em}}=-\frac{1}{2\epsilon_0 c}\frac{\partial P}{\partial t}. \tag{2}$$

The ρ_{ij} are the diagonal (populations) and off-diagonal elements (coherences) of the density matrix. They are damped by the phenomenological time constants T_1 and T_2, respectively. $\Omega(t)=E_{\mathrm{loc}}(t)\mu_{1S\text{-}2P}/\hbar$ is the instantaneous Rabi frequency. In the case of weak radiative coupling, $E_{\mathrm{loc}}(t)\approx E_{\mathrm{in}}(t)$ is a good approximation.[21] The present case, however, is in the strong radiative coupling limit, where the full expression for the local field[17] has to be applied $E_{\mathrm{loc}}(t)=E_{\mathrm{tr}}(t)=E_{\mathrm{in}}(t)+E_{\mathrm{em}}(t)$. The reemitted field $E_{\mathrm{em}}(t)$ is proportional to the time derivative of the macroscopic polarization $P(t)$, which in turn is proportional to the electric dipole moment $\mu_{1S\text{-}2P}=e\times 7.5$ nm and to the total sheet density $N_D d$ of coherently oscillating carriers. Radiative coupling has a strong impact on the dynamics of the system if the radiative coupling rate (in the linear case this is the radiative damping), $\Gamma_{\mathrm{rad}}=\omega_{1S\text{-}2P}N_D d\mu_{1S\text{-}2P}^2/(2\hbar\epsilon_0 c)=(5\ \mathrm{ps})^{-1}$ is higher than the irreversible decoherence rate described by T_2^{-1}. As a result, the entire ensemble of impurity transitions collectively acts with a much longer coherence time than that of the individual two-level system. In the Bloch vector picture for this case, the length of the Bloch vector remains almost constant and moves on the surface of the Bloch sphere.[25]

We numerically solved the Maxwell-Bloch equations [Eq. (2)]. The results are shown as the red/gray dashed lines in Figs. 3 and 4. We would like to stress that in the case of strong radiative coupling, i.e., $\Gamma_{\mathrm{rad}}\gg T_2^{-1}$, the relaxation processes described by the energy and phase relaxation times, T_1 and T_2, are of minor relevance. In this sense, the theoretical model does not contain any fitting parameters. Keeping this in mind, the quantitative agreement between experiment and theory is amazingly good. In particular, the theory quantitatively predicts the following experimental observations: (i) The phase and amplitude of the oscillations after the driving pulse, i.e., $E_{\mathrm{em}}(t>2\ \mathrm{ps})$. The long-lived macroscopic polarization occurs in the model only for strong radiative coupling. It should be noted that such behavior has not been predicted in Ref. 20, where any polaritonic features and their influence on the $1S$-$2P$ impurity absorption spectrum for high doping concentrations have been neglected. (ii) The maximal amplitude of the nonlinearly reemitted field, i.e., $E_{\mathrm{em}}(t)<N_D d\omega\mu_{1S\text{-}2P}/2\epsilon_0 c\approx 300\ \mathrm{V/cm}$, which occurs when all electrons coherently emit with the carrier frequency ω. (iii) The carrier-wave Rabi flopping regime in which the Rabi frequency is close to the carrier frequency of the driving pulse.[22] A characteristic feature is the oscillation at the third harmonic of the terahertz pulse observed during the driving pulse in Fig. 3(d). A similar phenomenon has been observed for interband polarizations of GaAs in the regime of carrier-wave Rabi oscillations.[23]

Finally, we discuss the energy transfer from a theoretical point of view [red/gray dashed lines in Figs. 4(b), 4(d), and 4(f)]. In the case of Rabi oscillations of a two-level system, the stored energy per carrier is given by the time-dependent excited state population $\rho_{22}(t)$ times the transition energy $\hbar\omega_{1S\text{-}2P}$. In Figs. 4(b), 4(d), and 4(f) we include the pulse area Θ of the Rabi oscillations calculated with our model. The model predicts the energy transfer quite well for pulse areas up to $\Theta\approx 2\pi$. For higher $E_{\mathrm{in}}(t)$ [Figs. 4(e) and 4(f)], the temporal phase of $I_{\mathrm{abs}}(t)$ and the amount of stored energy $\Lambda(t)$ are no longer correctly described by the Bloch equations [Eq. (2)]. At this point, the two-level approximation breaks down and, most probably, field ionization of neutral donor impurities[3] significantly alters the coherent nonlinear terahertz dynamics. For even higher applied fields [Fig. 3(e)], a clipping of the reemitted field amplitude (this is predicted for a two-level system) is no longer observed, pointing to a significant population of other levels in the conduction band continuum during the driving pulse.

IV. CONCLUSIONS

In conclusion, we studied the nonlinear terahertz response of a thin n-type GaAs layer at low lattice temperatures. The

emitted terahertz radiation is directly measured in phase-resolved nonlinear propagation experiments and demonstrates carrier-wave Rabi oscillations between bound levels of the shallow donor impurities. Sufficient radiative coupling between the impurity transitions makes it possible to observe coherently excited macroscopic $1S$-$2P$ polarizations oscillating for many picoseconds. The Rabi oscillation picture holds for driving fields below 5 kV/cm while for higher applied terahertz fields the two-level approach breaks down and field ionization processes of the neutral impurities come into play.

APPENDIX

In this Appendix, we briefly discuss two related phenomena occurring for intermediate doping concentrations: (i) the formation of impurity bands and (ii) the coupling between different $1S$-$2P$ transition dipoles within the system of neutral donors. In particular, we shall show that for the doping concentration studied here ($N_D=2\times10^{16}$ cm^{-3}), the two effects compensate each other to a large extent, resulting in a narrow $1S$-$2P$ absorption band as observed in our experiments (see Fig. 1).

For the doping density in our sample, the average distance between donors is around 37 nm, i.e., of the same order of magnitude as the Bohr radius. Thus, wave functions of neighboring impurities partially overlap, resulting in a delocalization of electron states.[16] A similar effect was observed for coupled intersubband transitions in semiconductor superlattices.[26] This tendency toward delocalization is partially compensated for by the Anderson localization[27] caused by the random distribution of impurities. Such an impurity band formation typically occurs around the doping density of our sample. Figure 5(b) shows the expected broadening of the $1S$ and $2P$ impurity bands as a function of the distance between charged donor sites. Because of the larger spatial extension of the $2P$ wave function, the broadening of the corresponding impurity band is stronger and occurs at larger distances than for the $1S$ band. A typical dispersion of the $1S$ and $2P$ impurity bands is shown in Fig. 5(a).[28] For vanishing disorder, optical transitions between occupied $1S$ and unoccupied $2P$ impurity band states will occur vertically (red/gray arrows). As a result, when considering two possible spin states for the electron, at $T=0$, the $1S$ impurity band is half filled. One expects a broadened and blueshifted $1S$-$2P$ absorption band.

For a doping concentration of the order of the Mott density,[12] which is the case for the sample studied here, the broadening turns out to be similar to the transition frequency, i.e., the $1S$ and $2P$ bands begin to overlap. Experimentally, however, we observe a rather narrow absorption line (Fig. 1). The coupling between different $1S$-$2P$ transition dipoles within the system of neutral donors is a counteracting effect to the formation of impurity bands, i.e., it results in a narrow collective response on the long-wavelength side of the broad band of uncoupled transitions. A similar effect was observed for coupled intersubband transitions.[29] The simplest theoretical model describing the dipole-dipole coupling is the frequency-dependent local field correction according to the Clausius-Mosotti relation. Applying this relation to the broad blueshifted absorption band [dashed line in Fig. 5(c)] of uncoupled transitions between the $1S$ and $2P$ impurity bands of our sample, one finds a much narrower and slightly blueshifted absorption line [solid line in Fig. 5(c)].

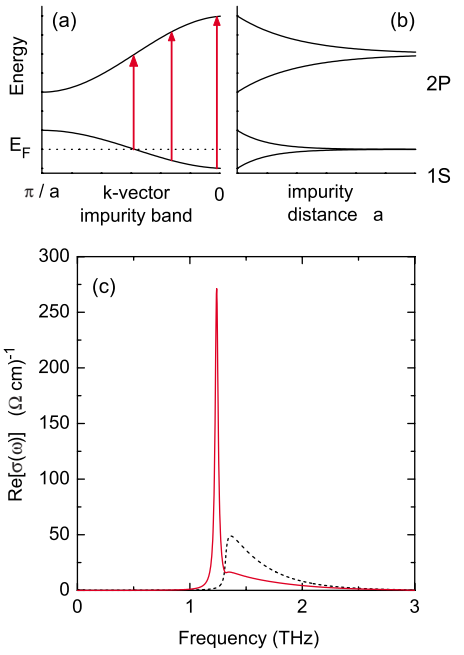

FIG. 5. (Color online) [(a) and (b)] Schematic of impurity band formation occurring at intermediate doping densities. (a) Dispersion of the $1S$ and $2P$ impurity bands expected for a crystal containing equally spaced charged impurities. Considering two possible spin states for the electron at $T=0$, the $1S$ impurity band is half-filled and optical transitions between occupied $1S$ and unoccupied $2P$ states vertically occur (red/gray arrows) resulting in a broadened and blueshifted absorption band. (b) Expected broadening of the $1S$ and $2P$ impurity bands as a function of the distance between charged donor sites. (c) Dashed line: calculated frequency-dependent conductivity for uncoupled transitions between the $1S$ and the $2P$ impurity band. Solid line: the local field correction according to the Clausius-Mossotti relation shows a pronounced coupling between different impurity transitions resulting in a narrow collective response on the red side of the broad band of uncoupled transitions (dashed line).

It should be noted that our experimental findings are in strong contrast to the absorption coefficients for a sample with $N_D=2\times10^{16}$ cm^{-3} reported in Ref. 20. The authors of Ref. 20 investigated a sample 100 times thicker than ours. We think that this fact hampers accurate quantitative transmission measurements. Furthermore, the analysis presented in Ref. 20 neglects the strongly frequency-dependent refractive index.

*reimann@bi-berlin.de
†woerner@mbi-berlin.de

[1] S. D. Ganichev and W. Prettl, *Intense Terahertz Excitation of Semiconductors* (Oxford University Press, Oxford, 2006).
[2] B. E. Cole, J. B. Williams, B. T. King, M. S. Sherwin, and C. R. Stanley, Nature (London) **410**, 60 (2001).
[3] P. Gaal, K. Reimann, M. Woerner, T. Elsaesser, R. Hey, and K. H. Ploog, Phys. Rev. Lett. **96**, 187402 (2006).
[4] R. A. Cooke, R. A. Hoult, R. F. Kirkman, and R. A. Stradling, J. Phys. D **11**, 945 (1978).
[5] I. Melngailis, G. E. Stillman, J. O. Dimmock, and C. M. Wolfe, Phys. Rev. Lett. **23**, 1111 (1969).
[6] K.-M. C. Fu, C. Santori, C. Stanley, M. C. Holland, and Y. Yamamoto, Phys. Rev. Lett. **95**, 187405 (2005).
[7] M. F. Doty, B. T. King, M. S. Sherwin, and C. R. Stanley, Phys. Rev. B **71**, 201201(R) (2005).
[8] S. G. Pavlov, R. K. Zhukavin, E. E. Orlova, V. N. Shastin, A. V. Kirsanov, H.-W. Hübers, K. Auen, and H. Riemann, Phys. Rev. Lett. **84**, 5220 (2000).
[9] D. G. Allen, M. S. Sherwin, and C. R. Stanley, Phys. Rev. B **72**, 035302 (2005).
[10] X. Hu, B. Koiller, and S. Das Sarma, Phys. Rev. B **71**, 235332 (2005).
[11] B. Koiller, X. Hu, and S. Das Sarma, Phys. Rev. B **73**, 045319 (2006).
[12] N. F. Mott, Rev. Mod. Phys. **40**, 677 (1968).
[13] Q. Wu and X.-C. Zhang, Appl. Phys. Lett. **71**, 1285 (1997).
[14] K. Reimann, Rep. Prog. Phys. **70**, 1597 (2007).
[15] J. J. LePore, J. Appl. Phys. **51**, 6441 (1980).
[16] F. Stern and R. M. Talley, Phys. Rev. **100**, 1638 (1955).
[17] T. Stroucken, A. Knorr, P. Thomas, and S. W. Koch, Phys. Rev. B **53**, 2026 (1996).
[18] S. Haas, T. Stroucken, M. Hübner, J. Kuhl, B. Grote, A. Knorr, F. Jahnke, S. W. Koch, R. Hey, and K. Ploog, Phys. Rev. B **57**, 14860 (1998).
[19] T. Shih, K. Reimann, M. Woerner, T. Elsaesser, I. Waldmüller, A. Knorr, R. Hey, and K. H. Ploog, Phys. Rev. B **72**, 195338 (2005).
[20] B. L. Cardozo, E. E. Haller, L. A. Reichertz, and J. W. Beeman, Appl. Phys. Lett. **83**, 3990 (2003).
[21] C. W. Luo, K. Reimann, M. Woerner, T. Elsaesser, R. Hey, and K. H. Ploog, Phys. Rev. Lett. **92**, 047402 (2004).
[22] S. Hughes, Phys. Rev. Lett. **81**, 3363 (1998).
[23] O. D. Mücke, T. Tritschler, M. Wegener, U. Morgner, and F. X. Kärtner, Phys. Rev. Lett. **87**, 057401 (2001).
[24] These frequency components lie in the gap of the ZnTe electro-optic detector, making an estimate of their absolute amplitude difficult.
[25] F. Bloch, Phys. Rev. **70**, 460 (1946).
[26] M. Helm, F. M. Peeters, F. DeRosa, E. Colas, J. P. Harbison, and L. T. Florez, Phys. Rev. B **43**, 13983 (1991).
[27] P. W. Anderson, Phys. Rev. **109**, 1492 (1958).
[28] J. C. Slater, Phys. Rev. **45**, 794 (1934).
[29] M. Zaluzny, Phys. Rev. B **49**, 2923 (1994).